PERGAMON

Planetary and Space Science 48 (2000) 331–339

Planetary and Space Science

The 90-day oscillations of Jupiter's Great Red Spot revisited

J.M. Trigo-Rodriguez[a], A. Sánchez-Lavega[b,*], J.M. Gómez[c], J. Lecacheux[d], F. Colas[e], I. Miyazaki[f]

[a]*Departamento Astronomía y Astrofísica, Universidad de Valencia, 46100 Burjassot, Valencia, Spain*
[b]*Departamento Física Aplicada I, E.T.S. Ingenieros, Universidad del País Vasco, Alda. Urquijo s/n, 48013, Bilbao, Spain*
[c]*Grup d'Estudis Astronomics, Barcelona, Spain*
[d]*Department Recherches Spatiales, Observatoire Paris, Meudon, France*
[e]*Bureau des Longitudes, Paris, France*
[f]*248-12 Akamichi, Gushikawa-shi, Okinawa, 904-22, Japan*

Received 29 July 1999; received in revised form 2 November 1999; accepted 29 November 1999

Abstract

We have analyzed a large set of ground-based CCD images covering the period from 1993 to early 1999, to address the current status and behavior of the 90-day longitudinal oscillations of the Jovian Great Red Spot (GRS). The good temporal sampling of these data have been complemented with a small set of high resolution Hubble Space Telescope images. The average zonal velocity of the GRS from 1994 to 1998 was -3.8 ms^{-1} with extreme values of -2.4 and -4.2 ms^{-1} in 1993–1994 resulting from the interactions with nearby features. Our study confirms the existence of the longitudinal oscillations with a mean period of 89.8 ± 0.15 days and an amplitude of $1.2 \pm 0.7^{\circ}$. The oscillations survived the strong interactions between the GRS and a variety of disturbances that took place during the observing period. No significant changes in the parameters defining the oscillations are observed when a comparison is made with a previous analysis from years 1961 to 1981.

Keywords: Jupiter; Atmosphere; Dynamics

1. Introduction

The Jovian Great Red Spot is the largest and long-lived vortex present in the atmospheres of the giant planets. It is the best studied from ground-based and spacecraft facilities, and represents the archetype of coherent and robust vortices formed in geophysical situations. Good knowledge of its fundamental properties is necessary to deepen insight on the origin of planetary vortices (Marcus, 1993). Among these properties the motions and interactions with close atmospheric features can be studied with ground-based facilities. Careful micrometer measurements of the GRS longitude position performed on photographic plates in the 1960s, showed that it exhibited quasi-sinusoidal oscillations with a period of about 90 days and $\sim 1.5^{\circ}$ peak-to-peak amplitude (Reese, 1972; Solberg, 1969). The oscillations were later measured independently in the 1970s on photographic plates by Gomez (1977) and by Guitar (1984) who re-measured the 1960s images and completed the analysis for a time span of 20 years (1961–1981).

However the oscillations are not easy to detect for several reasons: (i) the GRS as delineated by its topmost clouds is not a perfect oval, but its edges are irregular and change in time due to the interaction with neighboring features; (ii) the contrast of the GRS with the surrounding clouds depends on wavelength. It is high in violet-blue images where the GRS is dark, but low in red continuum where the GRS is clear because

* Corresponding author. Tel.: +34-946014255; fax: +34-946014178.
E-mail address: wupsalaa@bi.ehu.es (A. Sánchez-Lavega).

0032-0633/00/$20.00
PII: S0032-0633(00)00002-7

Table 1
Calendar of observations of Jupiter's Great Red Spot

Year	January	February	March	April	May	June	July	August	September	October	November	December
1993	3	–	–	9	14	10	5	–	–	–	–	–
1994	1	2	4	2	10	4	15	5	–	–	–	–
1995	1	2	6	4	7	4	8	4	1	3	8	1
1996	–	2	1	4	2	11	8	4	9	5	4	3
1997	–	3	–	8	11	9	15	5	9	7	4	2
1998	1	–	–	–	2	3	6	10	11	8	5	7
1999	2	1	–	–	–	–	–	–	–	–	–	–

of its red color. However it is conspicuous in the 890-nm methane band filter where the GRS detaches as bright because their cloud tops are highly placed relative to surroundings; (iii) the current size of the GRS is ~5 arc s and the oscillations represents maximum (peak to peak) displacements of ~0.3″; and (iv) the GRS interacts with nearby cloud systems and disturbances that change its motion in an unpredictable way masking the oscillatory behavior (see Rogers, 1995 for a review of these properties).

Because of these difficulties and due to the fact that the previous analyses were based on images taken with small aperture telescopes (30–61 cm) coupled to low resolution–few sensitive photographic plates, some doubts on the reality of the oscillations are raised. We thus decided to make a new analysis on this phenomenon, trying to separate the different types of motion present in the GRS and performing an accurate analysis and control of the measurement errors. Unfortunately the time span and coverage of the high resolution imaging performed by the spacecraft missions to Jupiter (Voyager 1 and 2 in 1979 and Galileo since 1995) is not good enough to recover the 90-day oscillations. Thus, regular ground-based observations are the best way to perform such analysis. The use of CCD imaging with its higher sensitivity, processing and measurement capability (because of the digital nature) represents the best choice. Its drawback lies in the low violet sensibility of common CCDs but this can be overcome using a blue filter (instead of violet), a 890-nm methane band filter, and near infrared continuum filters that overlap this band, increasing the contrast of the GRS in the Jovian disk.

2. Observations and analysis

This study covers the period January 1993–February 1999. Regular CCD images were taken with the 1-m Pic-du-Midi planetary dedicated telescope in France. They were complemented with sets obtained using smaller telescopes of 40–60 cm aperture under very good seeing conditions located in Japan, Spain, and USA. The wavelength coverage ranged from blue ($\lambda_{\text{eff}} \sim 400$ nm) to near-infrared ($\lambda_{\text{eff}} \sim 900$ nm). Broadband B, R and I filters and a narrow interference filter centered on the methane band at 890 nm were used (see Table 1 in Sanchez-Lavega et al., 1998 for details on filter characteristics).

In addition we used Hubble Space Telescope archived images obtained with the Wide Field-Planetary Cameras WFPC1 (few images in 1993) and WFPC2 (since 1994). The wavelength coverage was from the ultraviolet (336 nm) to the near infrared (953 nm), including again a methane band filter at 890 nm. The 336- and 890-nm images were used as a

calibration and quality control of the GRS positions determined with the ground based patrol. Fig. 1 is a mosaic of HST images of the GRS showing its aspect in violet and in the methane band in different dates of the observing period.

A total of 1100 images were selected, processed and analyzed for this study. Position measurements (longitude and latitude of the edges of the ellipse assumed to represent the shape of the GRS, see Fig. 1) were performed employing the LAIA software developed for planetary analysis in a PC environment (Cano, 1998). We covered 317 separate dates during the 1993–1999 period. A log of the observations (night coverage each month) is given in Table 1.

There are two main types of errors in our measurements. (1) Those introduced during the limb fit procedure (''navigation'') to generate the ellipse that represents the jovian disk projected on the sky. (2) The cursor pointing on the edges (north, south, east and west) of the ellipse that represents the GRS. The limb fit is performed automatically by LAIA routines that search for the gradient of intensity around a point marked with the cursor close to the limb. This step is repeated with a series of trial points along the disk, so LAIA finally fits automatically the ellipse to the limb. The cursor pointing on the GRS edges is manual and its positioning depends on where the operator judges the edge is located. It is something subjective, since normally the edges of the GRS are not sharp enough because of the existence of turbulence and cloud heterogeneity, except along the southern edge that is usually delineated by a dark border (Fig. 1). To reduce this error, at least three independent measurements were performed on each edge of the GRS in every image. Considering the navigation and edge positioning errors, we find an average standard deviation of $\pm 0.39^{\circ}$ in the longitude and $\pm 0.52^{\circ}$ in the latitude position measurements of the GRS. This difference between longitude and latitude errors comes in part from the difference between the polar and equatorial radius of Jupiter, and in differences in the sharpness showed by the East–West and North–South extremities of the GRS (i.e. to differences in contrast). Latitudes are planetographic and longitude positions are

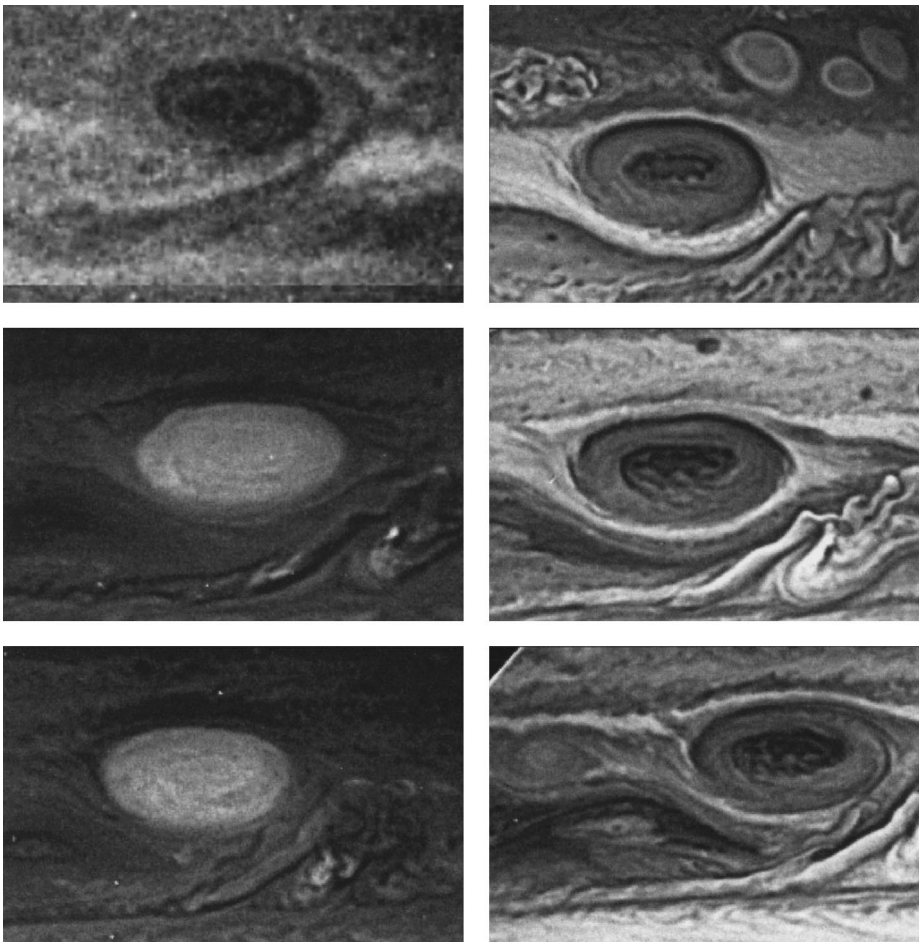

Fig. 1. Hubble Space Telescope images of the Jovian Great Red Spot (from top, left to right, to bottom): 31 July 1993 (violet, it shows a STrZ disturbance), 17 February 1995 (blue), 21 October 1996 (methane, 890 nm), 21 October 1996 (blue), 4 April 1997 (methane, 890-nm), 4 April 1997 (blue, it shows the WTrO to the left of the GRS). Telescopic view is presented with south up and east to the left.

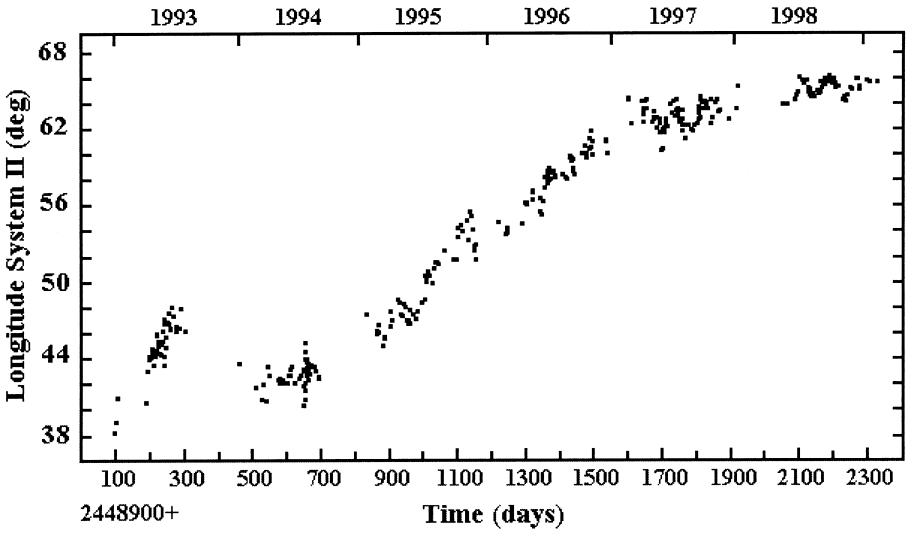

Fig. 2. Motion of the GRS in System II longitudes during the period January 1993–February 1999.

given in System II (defined by a rotation rate $\Omega_{II} = 870.27°$/day). We have chosen this System both for historical reasons (to aid a comparison with the Solberg and Reese's data) and because the GRS remains "quasi-stationary" on it.

3. Results

Fig. 2 shows the drift in System II longitudes. Inspection of this graph shows evidence of oscillations of the GRS center from 1996 to 1999 (JD > 2450100). In other epochs, as during 1993–1994, no evidence of oscillations were seen at all (JD < 2449600). Fig. 3 shows the latitude position of the GRS along this period. The data are noisy and there is no evidence of any regular oscillation in latitude. A periodogram of this plot shows no clear frequency peaks except the alias of the synodic period. To better characterize the GRS, we have used the high quality HST images (1993–1997) to obtain its size and mean latitude (Table 2). These values are in agreement with similar measurements based on Voyager 1 and 2 images in 1979 by Sada et al. (1996) and on recent Galileo images by Vasavada et al. (1998) and suggest that the GRS has stabilized its size during the last 20 years.

3.1. Mean and fluctuating motion of the GRS

The mean zonal motion of the GRS in System II

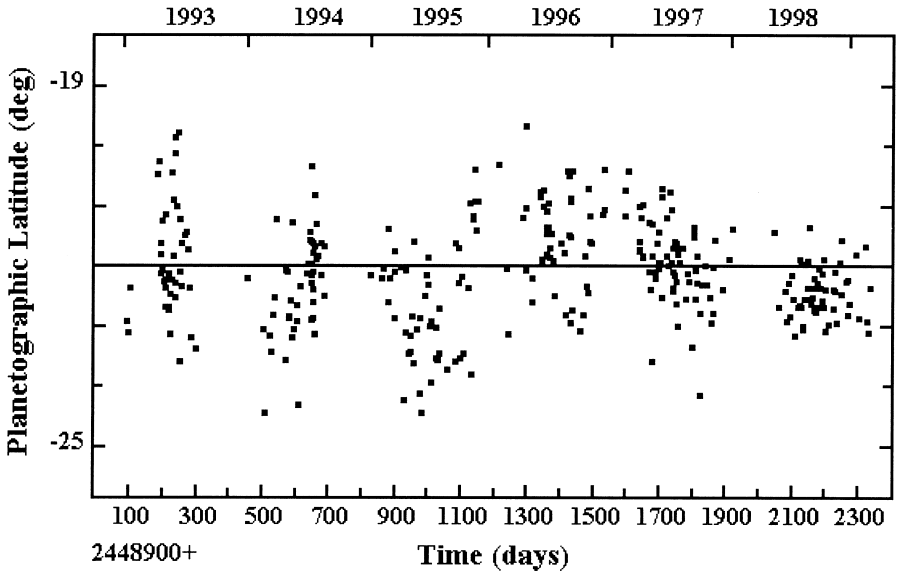

Fig. 3. Planetographic latitude of the center of the GRS during the period January 1993–February 1999.

longitude has been obtained from a fit to the drift curve in Fig. 2 (period 1994–1998) to a second order polynomial:

$$\lambda(t) = 31.43^\circ + 0.02134(^\circ/\text{day})t - 9.32 \times 10^{-7}(^\circ/\text{day}^2)t^2 \quad (1)$$

where λ is the longitude and the time $t = 0$ is the elapsed time in days from the Julian Date 2449000. The mean drift can be easily converted to an average zonal velocity relative to the internal rotation frame System III ($\Omega_{III} = 870.536^\circ$/day) of -3.8 ms^{-1}.

Superposed to this steady motion there are irregular fluctuations and the oscillations (Fig. 2). The irregular motion occurred essentially in 1993 and corresponds to a period when the GRS interacted strongly with a South Equatorial Belt Disturbance and with a South Tropical Disturbance (Sanchez-Lavega et al., 1996). This last feature is prominent in Fig. 1 (31 July 1993) where it detaches as a large dark arc encircling half the perimeter of the GRS. As a consequence of these interactions, the zonal velocity of the GRS changed from $u = -4.2$ ms^{-1} (JD = 2448998–2449160) to $u = -2.4$ ms^{-1} (JD = 2449160–2449181). Another important interaction took place in May 1997 when the GRS encountered a large vortex (the White Tropical Oval) in the STrZ shown also in Fig. 1 (4 April 1997) (Sanchez-Lavega et al., 1998). This interaction gave rise to a short-term (7–10 days) fluctuation in the GRS motion whose details are given in Sanchez-Lavega et al. (1998). It is evident that these types of interactions mask the otherwise regular oscillations of the GRS described below.

3.2. The 90-day oscillation

To analyze the oscillations with more detail, we have performed a linear fit to a straight line of the drift motion of the GRS in some temporal segments typically covering one apparition. We then calculate the longitude residuals from this linear fit. The detrended longitudes are used as the input data to determine the characteristics of the oscillations (Fig. 4).

Periodograms of the GRS motion were generated for the whole observing period and for selected temporal intervals. Because the observation times are unevenly spaced, we used different tools in the periodogram analysis, basically a Discrete Fourier Transform (DFT; see Deeming, 1975), a Phase Dispersion Minimization procedure (PDM, Stellingwerf, 1978) and the method of Scargle (1982). Fig. 5 shows the periodogram using the DFT for the period January 1995–February 1999 when the oscillations became more apparent. Regardless of the procedure employed, the only oscillatory component in evidence for the GRS is the 90-day oscillation. Aliases (i.e. frequency combinations) of the 400-day synodic period of Jupiter (intervals between conjunctions of Jupiter and the Sun) flank the central peak, and subarmonics of the 90-day oscillation are seen with increasing frequencies from the peak. Fig. 6 shows the oscillating motion in phase for this temporal interval. The peak defining the oscillation is clean and well defined. The final characteristics of the oscillations from this analysis are given in Table 2. Our period is close to that obtained by Reese (1972) of 89.89 days and by Guitar (1984) of 89.93 days. Similarly, our amplitude (peak to peak) is within the values quoted by Guitar of 1.06° and Reese of 1.54°.

The maximum drift rate produced by the oscillation is $\omega = A(2\pi/P)$ and this represents a maximum zonal velocity change of $\sim$1.8 ms^{-1} with the above parameters. This velocity change is greater than the velocity changes resulting from interactions and indicates

Table 2
Measured parameters of the GRS from 1993 to 1999

Location and size (n is the number of individual images measured)	
Average planetographic latitude of the GRS center	$-22.26^\circ \pm 0.57^\circ$ ($n = 43$)
Zonal size	$18.07^\circ \pm 0.91^\circ$ ($n = 46$)
Meridional size	$10.44^\circ \pm 0.59^\circ$ ($n = 47$)
Aspect ratio (Meridional size (degrees)/Zonal size (degrees))	0.578 ± 0.054
Motions	
Zonal average velocity (relative to System III)	-3.8 ms^{-1}
Zonal velocity fluctuation (interactions, relative System III)	-2.4 to -4.2 ms^{-1}
Meridional velocity	undetected
Longitudinal oscillations	
Period P	89.8 ± 0.15 days
Amplitude (peak to peak) A	$1.2 \pm 0.7^\circ$
Ephemeris for the oscillation maximum	
JD (max) = 2451087.5 ($\pm$1.5) + 89.8 ($\pm$0.15) n, ($n = 0, \pm 1, \pm 2, \pm 3, \ldots$)	

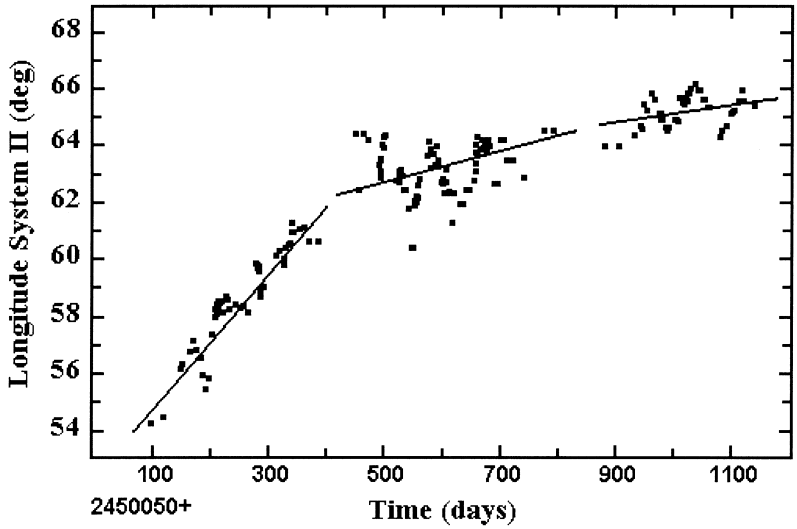

Fig. 4. Deviations in the longitude position of the center of the GRS with respect to its mean motion during the apparitions of 1996 (first segment), 1997 (second segment) and 1998 (third segment).

the dynamical importance of the oscillations in the GRS motion.

4. Discussion

The mean velocity of the GRS for this period was determined to be -3.8 ms^{-1}. If we assume this velocity to be that of the center of the GRS, as determined by the cloud patterns (located at $-22.3°$), then a significant difference is found when comparing it with the mean zonal flow velocity of -27.9 ms^{-1} measured at the $-22.3°$ latitude by Limaye (1986). In such a case the GRS should not be advected by the flow, but moving with a velocity of about $+20$ ms^{-1} eastward relative to the mean flow (see e.g. Achterberg and Ingersoll, 1994). On the other hand, the measured velocity of the GRS corresponds in Limaye's profile to the latitude $-23.5°$. An alternative explanation is to assume that the GRS is in fact advected by the flow

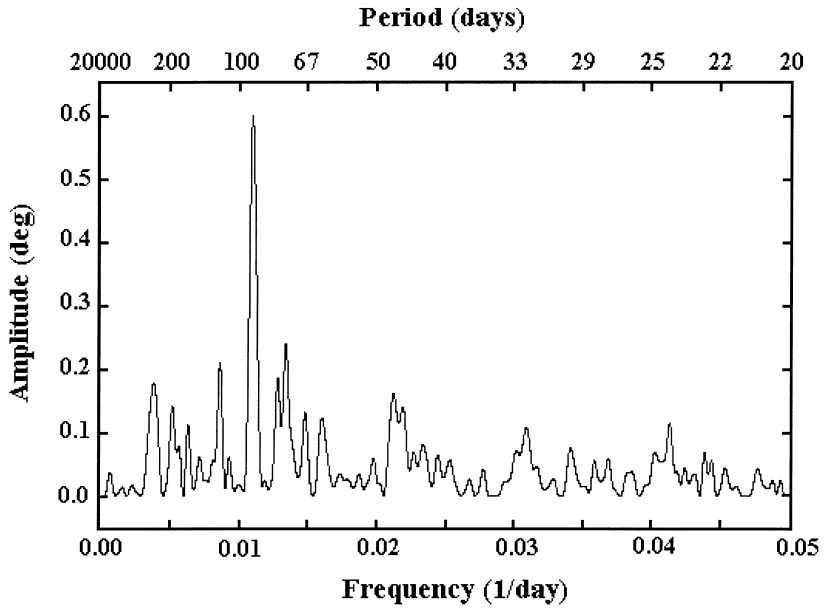

Fig. 5. Periodogram of the linear detrended longitude residuals of the GRS motion from January 1995 to February 1999. The 90-day oscillation is clean and flanked by aliases of the 400-day synodic period and to the left by sub-harmonics of the 90-day oscillation. The frequency and the corresponding period (1/frequency) are indicated in the lower and upper abscissa, respectively.

but that the effective dynamic "guiding" center of the GRS is displaced ~1.2° southward of its geometric center.

Numerical models that represent the characteristics of the GRS try in general to reproduce their motions. It is generally believed that the GRS velocity departure from the ambient mean flow velocity is related to the nature of the vortex itself. For example, quasigeostrophic models that represent the GRS as a finite-patch of potential vorticity $q(x, y)$ with circulation concentrated in a peripheric ring, predict that its motion takes place with the local velocity averaged over its area (Marcus, 1993). The GRS average zonal velocity is then given by

$$u_{\mathrm{GRS}} = \frac{\iint q(x, y)[\langle v_x(y)\rangle + v'_x(x, y, t)]\,\mathrm{d}x\,\mathrm{d}y}{\iint q(x, y)\,\mathrm{d}x\,\mathrm{d}y} = \langle u_{\mathrm{GRS}}\rangle + u'_{\mathrm{GRS}} \quad (2)$$

Here (x, y) are the horizontal longitude and latitude coordinates, $\langle v_x(y)\rangle$ is the average (time-independent and x-independent) zonal component of the flow velocity and $v'_x(x, y, t)$ its time-dependent correction (Marcus, 1993). Using the potential vorticity measurements within the GRS of Dowling and Ingersoll (1989), Marcus derived from Eq. (2) that $u_{\mathrm{GRS}} = -1 \pm 8\ \mathrm{ms}^{-1}$. The velocity uncertainty comes from a 25% uncertainty in the measurement of $q(x, y)$. Note however, that this value encompasses our precise measurement of $-3.8\ \mathrm{ms}^{-1}$. The contribution of the second term in Eq. (2) is probably small (Marcus, 1993). However this term represents the advection due to neighboring patches of vorticity and the velocity due to the boundaries (Marcus, 1993). It could represent the contribution to the GRS motion produced by the interaction with nearby features and give account of the range of velocities measured during such interactions (namely $-2.4\ \mathrm{ms}^{-1}$ to $-4.2\ \mathrm{ms}^{-1}$). In such a case, our data suggest that $\langle u_{\mathrm{GRS}}\rangle = -3.8\ \mathrm{ms}^{-1}$ and $u'_{\mathrm{GRS}} = +1.4$ to $-0.4\ \mathrm{ms}^{-1}$. This second term could also be involved in the GRS oscillations. However is it difficult to see how a regular motion as the 90-day oscillations can be maintained in such a way during long temporal intervals (a periodic source of vorticity should be required to feed the GRS).

On the other hand, quasigeostrophic and intermediate geostrophic Rossby vortices in a shear flow and on a β plane under a variety of circumstances have been proposed to simulate the GRS characteristics (see e.g. Achterberg and Ingersoll, 1994; Nezlin and Snezhkin, 1993; Williams, 1996, 1997; Williams and Wilson, 1988). In their simple form, Rossby vortices are expected to move with a maximum velocity

$$u + -\beta L_{\mathrm{R}}^2 \quad (3)$$

Here L_{R} is the deformation Rossby radius and $\beta = (2\Omega \cos\varphi)/R$ with R being the Jovian radius. At the latitude of the GRS $\beta = 4.5 \times 10^{-12}\ \mathrm{m}^{-1}\ \mathrm{s}^{-1}$. With the measured mean value for the GRS speed of $-3.8\ \mathrm{ms}^{-1}$, a deformation scale $L_{\mathrm{R}} = (u/\beta)^{1/2} = 914$ km is obtained according to Eq. (3). It is interesting that the context of the Rossby wave hypothesis the results of the numerical model by Williams (1997) that uses a similar value of the deformation scale. He predicts longitudinal oscillations of the GRS as a result of the recurring interaction between the vortex and a wave disturbance that his model induces in the neighboring westerly jet at −25° latitude (see his Fig. 5).

Other simple hypotheses for this oscillation not related to the GRS itself could be the following. (1) Peri-

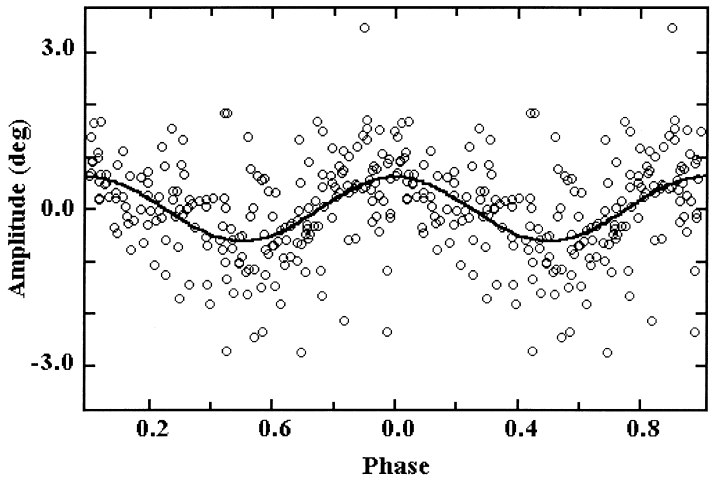

Fig. 6. Oscillations in phase of the GRS center longitude for the period January 1995–February 1999. Two oscillations have been included for clarity.

odic (90-day) encounter between the GRS and a Jovian feature that could act as a "forcing" mechanism. This requires the feature to move with a zonal velocity of $|u| = 2\pi R \cos\varphi / P \sim 55$ ms^{-1} relative to the GRS. According to Limaye's profile, the flow velocity at the southern edge of the GRS is ~ 42 ms^{-1} (i.e. a velocity relative to the GRS of $\sim +38$ ms^{-1}, equivalent to an encounter period of 125 days). Similarly at the northern boundary the flow has a velocity of -55 ms^{-1} (i.e. a velocity relative to the GRS of ~ -59 ms^{-1}, equivalent to an encounter period of 81 days). Although these values are not far away of the 90-day period, there is no observational evidence of such permanent forcing feature either in the northern or in the southern flanks. (2) Coupled oscillations in latitude or altitude in the presence of wind shear. However, there is no evidence of meridional oscillations in our data (see Fig. 3) as we presented previously. Using Limaye's zonal wind profile and our value of 1.8 ms^{-1} for the GRS velocity component due to the oscillation, a latitude variation of 0.16° should be necessary to produce the oscillation. This value is below our measured error bar latitude so no conclusion can be reached. In any case, the problem would subsist since it would be necessary to find the source of the meridional changes. Finally, variations in the altitude of the vortex have also been suggested to be in the origin of the oscillations (Achterberg and Ingersoll, 1994), but at present this effect cannot be tested.

Finally, using the ephemeris equation in Table 2, we have checked the possibility that the 1995–1999 oscillations were in or out of phase with those reported by Reese (1972) and Guitar (1984). In fact Guitar stresses that the phase remained essentially invariant during his 20 years of observations. It is striking to see that the maximum given by Reese's ephemeris equation on JD = 2440763 can be recovered within 3 days with our equation and $n = -115$. Although most probably this represents a coincidence, this aspect merits to be checked in the future.

5. Conclusions

A 6-year analysis of CCD images using ground-based facilities supported by Hubble Space Telescope imaging, confirms the existence in modern times of the GRS 90-day zonal oscillations. Their properties (period, amplitude and phase) have changed little between the 1961 and 1981 period of previous analysis and present times (1993–1999). The motion of the GRS can be resolved in three adding components. (1) A zonal "steady" velocity of ~ -3.8 ms^{-1} (prevailing at least since the 1940s according to Rogers, 1995). (2) A quasi-sinusoidal oscillation (period ~ 89.8 days and amplitude $\sim 1.2°$). (3) A "fluctuating" or time-dependent term introduced via the interactions of the GRS with nearby features (maximum short-term velocity departures from the mean of $\sim +1.4$ to -0.4 ms^{-1}). Any comprehensive model of the GRS should incorporate the peculiarities of such motions and interactions. Continuous long-term observations on this topic should address the question of the phase preservation of the oscillations and the tentative slow changing period. Detailed observations with modern facilities of the motions of other giant planet vortices as for example those of Jupiter, or Saturn (with the Cassini mission), or with ground-based and HST telescopes in Neptune (see e.g. Sromovsky et al., 1993), would help to understand their nature.

Acknowledgements

The Spanish team was supported by Gobierno Vasco research grant 1997/34. We thank J. A. Cano (GEA, Spain) for the development of the image processing software LAIA, and R. Barberá for the software AVE, and G. Domínguez for preparing the data base. We acknowledge the Space Telescope Science Institute and the ESO ST-ECF archive facilities for supplying us with the Hubble Space Telescope images.

References

Achterberg, R.K., Ingersoll, A.P., 1994. Numerical simulation of baroclinic Jovian vortices. J. Atmos. Sci. 51, 541–562.

Cano, J.A., 1998. L.A.I.A.: "Laboratorio de Análisis de Imágenes Astronómicas". Grup d'Estudis Astronomics, Barcelona (Spain).

Deeming, T.J., 1975. Fourier analysis with unequally-spaced data. Astrophys. Space Sci. 36, 137–158.

Dowling, T.E., Ingersoll, A.P., 1989. Jupiter's Great Red Spot as a shallow water system. J. Atmos. Sci. 46, 3256–3278.

Gomez, J.M., 1977. Jupiter: Estudio de las evoluciones de la Mancha Roja. Presentaciones de 1974–75 y 1975–76. Astrum 37, 3–34 (in spanish).

Guitar, H., 1984. Analysis of motions of Jupiter's Great Red Spot and White Ovals. PhD Thesis, New Mexico State University.

Limaye, S.S., 1986. Jupiter: new estimates of the mean zonal flow at the cloud level. Icarus 65, 335–352.

Marcus, P.S., 1993. Jupiter's Great Red Spot and other vortices. Annu. Rev. Astron. Astrophys. 31, 523–573.

Nezlin, M.V., Snezhkin, E.N., 1993, Rossby Vortices, Spiral Structures, Solitons, Springer Series in Nonlinear Dynamics, Springer-Verlag, Heidelberg.

Reese, E.J., 1972. Jupiter: its Red Spot and disturbances in 1970–1971. Icarus 17, 57–72.

Rogers, J.H., 1995. The Giant Planet Jupiter. Cambridge University Press, Cambridge, UK.

Sada, P.V., Beebe, R.F., Conrath, B.J., 1996. Comparison of the structure and dynamics of Jupiter's Great Red Spot between the Voyager 1 and 2 encounters. Icarus 119, 311–335.

Sanchez-Lavega, A., Gomez, J.M., Lecacheux, J., Colas, F., Miyazaki, I., Parker, D., Guarro, J., 1996. The South Equatorial Belt of Jupiter, II: the onset and development of the 1993 disturbance. Icarus 121, 18–29.

Sanchez-Lavega, A., Hueso, R., Lecacheux, J., Colas, F., Rojas, J.F., Gomez, J.M., Miyazaki, I., Parker, D., 1998. Dynamics and interactions between a large-scale vortex and the Great Red Spot in Jupiter. Icarus 136, 14–26.

Scargle, J.D., 1982. Studies in astronomical time series analysis. II. Statistical aspects of spectral analysis of unevenly spaced data. Astrophys. J. 263, 835–853.

Solberg, H.G., 1969. A 3-month oscillation in the longitude of Jupiter's Red Spot. Planet. Space Sci. 17, 1573–1580.

Sromovsky, L.A., Limaye, S.S., Fry, P.M., 1993. Dynamics of Neptune's major cloud features. Icarus 105, 110–141.

Stellingwerf, R.F., 1978. Period determination using phase dispersion minimization. Astrphys. J. 224, 953–960.

Vasavada, A.R., Ingersoll, A.P., Banfield, D., Bell, M., Gierasch, P.J., Belton, M.J.S., et al., 1998. Galileo imaging of Jupiter's atmosphere: the Great Red Spot, Equatorial Region and White Ovals. Icarus 135, 265–275.

Williams, G.P., Wilson, R.J., 1988. The stability and genesis of Rossby vortices. J. Atmos. Sci. 45, 207–241.

Williams, G.P., 1996. Jovian dynamics. Part I: vortex stability, structure and genesis. J. Atmos. Sci. 53, 2685–2734.

Williams, G.P., 1997. Planetary vortices and Jupiter's vertical structure. J. Geophys. Res. 102, 9303–9308.